Wheelflat impact noise prediction using detailed contact model

Jiannan Yang, David Thompson

Wheelflat impact noise prediction using detailed contact model

J. Yang and D. J. Thompson

Dynamics Group-ISVR - University of Southampton, University Road, SO17 1BJ Southampton, UK
jny1e08@soton.ac.uk

Wheel/rail impact noise, which has a similar excitation mechanism to rolling noise, is caused by rail and wheel discontinuities. However, the Hertzian contact model requirements are not fulfilled due to the large variation of the geometry in the wheel flat area. Therefore, a detailed numerical contact model has to be implemented dynamically in the wheel/rail interaction to predict the impact vibration due to wheel flat in time domain. The contact patch size is discretized adaptively at each time step to ensure that all the contact points are included. Roughness input data from SNCF field measurements on a wheel flat are used to validate the model in terms of track vibration during pass-by. The Hertzian spring is also compared with the new detailed contact model in terms of contact force and rail response.

1 Introduction

Impact noise, which has a similar excitation mechanism to rolling noise, is caused by rail and wheel discontinuities [1]. Big reductions in impact noise have been achieved by using welded rails, but wheel flats, switches and insulated joints still remain important sources of noise. In [2], Newton and Clark performed a test to investigate the dynamic effects of wheel flats. The difficulty of locating the flat relative to the instrumentation was avoided by placing an equivalent indentation on the railhead.

A hybrid method was adopted by Wu and Thompson in [3] to predict wheel flat impact noise. The contact force found in the time domain using a simple rail/wheel model was transformed to an equivalent roughness spectrum, and the equivalent roughness was then used as input to the Track-Wheel Interaction Noise Software (TWINS) [4] to predict the impact noise from wheel flats.

A Hertzian contact model has mostly been used in predicting the response to wheel flats. This could be misleading as the geometry variations are very large in the wheel flat area so that the surface cannot be approximated by a quadratic Hertz profile any more. Baeza et al [5] have employed a numerical non-Hertzian contact model to study the impacts from theoretical fresh or rounded wheel flats. The relation between the contact force and the relative approach of wheel and rail in the wheel flat area was pre-processed and stored as a large look-up table. This table was then used in combination with wheel and rail dynamics at each time step of the train movement for contact force prediction. It was found that Hertz contact tends to overestimate the peak impact force. However, as the contact force at the wheel flat has a large dynamic range, the look-up table has to be big enough to include all possible values.

In this paper, a numerical non-Hertzian contact model is included dynamically in the interaction calculation at each step. Measured wheel flat geometry is studied and the pass-by vibration is compared with measurement. A Hertzian contact model is also considered for comparison and it is shown that the improvement of using the detailed contact model for wheel flat impact analysis is significant.

2 Wheel/rail interaction

The interaction model used here is derived from [6, 7]. The track is modelled using Finite Element method with the rail represented by Timoshenko beam elements, see Figure 1. The vehicle is simplified to a preload and wheel mass. The track and wheel are coupled by the contact force and the equations of motion of the system are solved using a state space approach in time domain.

However, some adjustment have to be made. First, in [6, 7] roughness and its derivatives are the input to the system. But as the wheel and rail are in contact over an area, it is difficult to decide how to process the measured roughness. The equivalent roughness under nominal preload could be used in line with a contact spring model [8]. But for the wheel flat area, the real roughness could deviate significantly from the equivalent roughness under preload. Second, the contact force is output in the form of impulse and that makes it difficult to couple the numerical contact model to the interaction calculation. Here, the force itself is computed in each step, but due to the nature of the time stepping integration, no direct output of the contact force from the calculation is obtained. Instead the contact force is calculated in a post-processing step from the wheel motion, see Section 6.

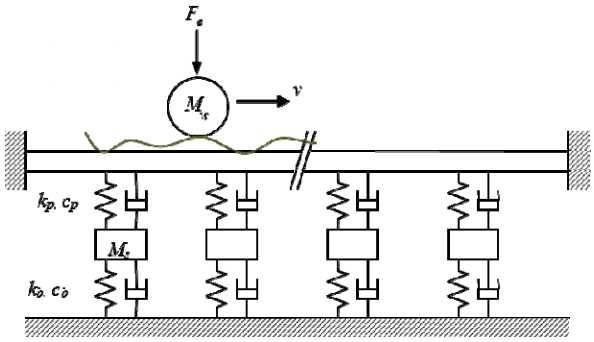

Figure 1 Wheel/rail interaction model

The equation of motion for the track can be arranged to a first order system form as

$$\mathbf{A}_T\dot{\mathbf{y}} + \mathbf{B}_T\mathbf{y} = \mathbf{f}_T \tag{1}$$

$$\mathbf{A}_T = \begin{bmatrix} \mathbf{C} & \mathbf{M} \\ \mathbf{M} & \mathbf{0} \end{bmatrix} \quad \mathbf{B}_T = \begin{bmatrix} \mathbf{K} & \mathbf{0} \\ \mathbf{0} & -\mathbf{M} \end{bmatrix} \quad \mathbf{y} = \begin{Bmatrix} \mathbf{u} \\ \dot{\mathbf{u}} \end{Bmatrix} \quad \mathbf{f}_T = \begin{Bmatrix} \mathbf{f} \\ \mathbf{0} \end{Bmatrix} \tag{2}$$

where **M**, **C** and **K** are the global mass, damping and stiffness matrices, while **u** and **f** are vectors of displacements and forces.

The motion of the track in modal coordinates is

$$\mathbf{a}_T\dot{\mathbf{q}} + \mathbf{b}_T\mathbf{q} = \mathbf{Q} \tag{3}$$

$$\begin{aligned} \mathbf{y} &= \mathbf{P}\mathbf{q} \\ \mathbf{Q} &= \mathbf{P}^T\mathbf{f}_T \end{aligned} \tag{4}$$

where **q** is the modal coordinate vector and **Q** is the modal load vector. **P** is the complex modal matrix containing eigenvectors as its columns. The system matrices in modal form are

$$\mathbf{a_T} = \mathbf{P^T A_T P};\ \mathbf{b_T} = \mathbf{P^T B_T P} \tag{5}$$

The equations of motion of the vehicle could be assembled in a similar manner as the track, but it is simplified to a single wheel here. Therefore the interaction motion between the wheel and rail can be described in a compact first order form as

$$\mathbf{A\dot{g} + Bg = F} \tag{6}$$

The system matrices **A** and **B** are

$$\mathbf{A} = \begin{bmatrix} \mathbf{a_T} & \mathbf{0} & \mathbf{0} \\ \mathbf{0} & 1 & M_w \\ \mathbf{0} & 1 & 0 \end{bmatrix}; \mathbf{B} = \begin{bmatrix} \mathbf{b_T} & \mathbf{0} & \mathbf{0} \\ \mathbf{0} & 0 & -1 \\ \mathbf{0} & 0 & -1 \end{bmatrix} \tag{7}$$

The coordinates and force vector are

$$\mathbf{g} = \{\mathbf{q} \quad u_w \quad \dot{u}_w\}^{\mathbf{T}} \tag{8}$$

$$\mathbf{F} = \{\mathbf{Q} \quad F_e - F_c \quad 0\}^{\mathbf{T}} \tag{9}$$

where u_w and M_w represent the wheel displacement and mass, while the track is included in its modal form.

The contact force at each time step is calculated from the relative displacement of wheel and rail from the previous step. It also depends on the surface profile at that position. This will be explained in detail in section 4.

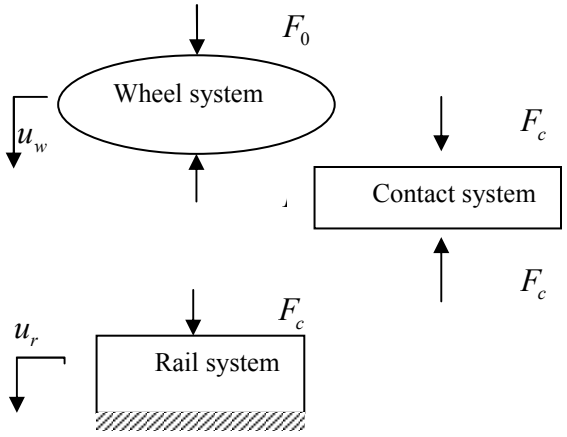

Figure 2: system view of the interaction

3 Hertzian contact model

As shown in Figure 2, the wheel and rail are coupled by the contact system. Hertz contact is a special case where the contact system can be described as a spring with constant non-linear stiffness. The Hertzian contact force is

$$\begin{cases} F_c = C_H (u_w - u_r - r)^{3/2} & u_w - u_r - r > 0 \\ F_c = 0 & else \end{cases} \tag{10}$$

where C_H is the Hertzian constant depending on the radius of curvature of the contact and material properties. u_w and u_r are the displacements at degrees of contact force. r represents the surface roughness.

However, as the wheel flat geometry varies rapidly around the contact area, C_H is not a constant as the wheel moves along the rail and a non-Hertzian contact model should be employed.

4 Non-Hertzian contact model

For normal contact problems, the displacement on the surface can be computed as:

$$u(x,y) = \iint_{\text{contact area}} A(\xi,\eta;x,y)\, p(\xi,\eta) d\xi d\eta \tag{11}$$

where (ξ,η) are the coordinates for the contact region and (x,y) are for the whole surface. $A(\xi,\eta;x,y)$ is the displacement at (x,y) due to a point load at (ξ,η) and is called the influence function. By assuming the two bodies in contact can be approximated by a half-space, the influence function is explicitly known [9].

Due to the existence of roughness between the wheel and rail, especially at the wheel flat area, where the radius of the curvature at the contact asperities might be comparable to the contact size, the half-space assumption is not fully justified. However, as the essence of the half-space assumption is that approach of the two contact bodies is not affected by the local deformation [10], in railway applications, half-space theory is generally valid unless flange contact occurs, where the thickness of the wheel flange is comparable to the contact size. Therefore, half-space theory is still employed here.

Although the pressure distribution is not known, for two bodies in contact, the surface displacements satisfy the boundary condition within the contact area:

$$u(x,y) = u_w - u_r - h(x,y) \tag{12}$$

where $u_w - u_r$ is the relative displacement of wheel and rail and $h(x,y)$ is the profile difference. The profile difference describes the geometry of the surfaces of the two bodies in contact (including roughness) and will be explained in detail in section 5.

Equations (11) and (12) form a boundary value problem, which is difficult to solve analytically. Therefore, a numerical method is adopted. The Matrix Inversion method [11] is employed here, which involves inverting the matrix of influence coefficients.

The contact area is discretised and piecewise constant pressure element is assumed, which according to [9] has about the same accuracy as piecewise linear pressure elements in terms of surface displacement. If there are N elements in contact, equation (11) and (12) is discretised to

$$\sum_{j=1}^{N} A_{ij} p_j = u_w - u_r - h_i \tag{13}$$

where A_{ij} can be found in [7, 9, 11]. As the contact area is not known, the calculation has to be done iteratively.

The algorithm to calculate the contact force is implemented as shown in Figure 3. The minimum of the profile difference between wheel and rail is set as the centre of the contact patch grid. The potential contact area (PCA) is first estimated as the inter-penetration region based on the relative wheel and rail displacement from the previous

step. The trial grid size is made large to ensure that the inter-penetration region is contained. The influence matrix **A** can then be formed for the PCA and the pressure follows from the inversion process. The pressures are checked for any tensions and these are eliminated where applicable. After removing all tensions, the pressures are checked to make sure they are zero at the boundaries of the contact area. Otherwise, the PCA is enlarged and the calculation is repeated with the new contact area. The contact force is the sum of the pressures times the area A_c at points in contact.

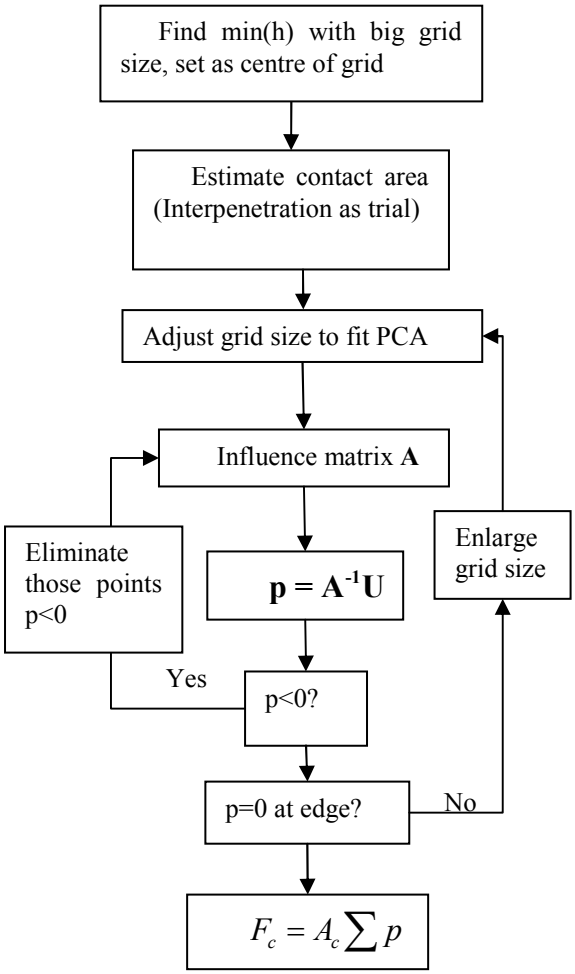

Figure 3 Adaptive algorithm for computing of contact force

To couple the contact force calculation to the interaction of the wheel and rail, the relative displacement of wheel and rail $u_w - u_r$ and the profile difference h are the input to the contact model described above at each time step. The resultant contact force is then the input to equation (9) for the interaction calculations.

5 Measured wheel flat geometry

Rather than using a theoretical shape approximating a wheel flat, the measured geometry from a wheel with a flat spot is investigated [12]. The surface roughness was measured along 12 different lines in the transverse direction on the wheel with a flat spot, as shown in Figure 4. The roughness is sampled at 1 mm intervals both in circumferential and transverse directions. The wheel and rail smooth transverse profiles are normalized to the nominal contact point which is determined as the geometrical stable running position [13]. By superimposing the measured roughness on to the smooth transverse profile of the wheel, a 3D mapping of the wheel surface geometry can be obtained and is shown in Figure 5.

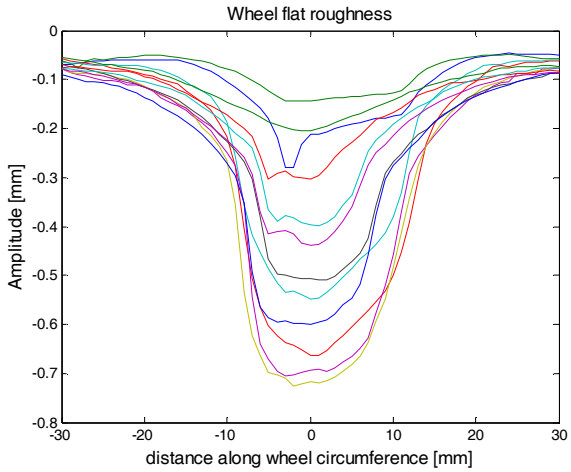

Figure 4: Wheel flat roughness amplitude along wheel circumference

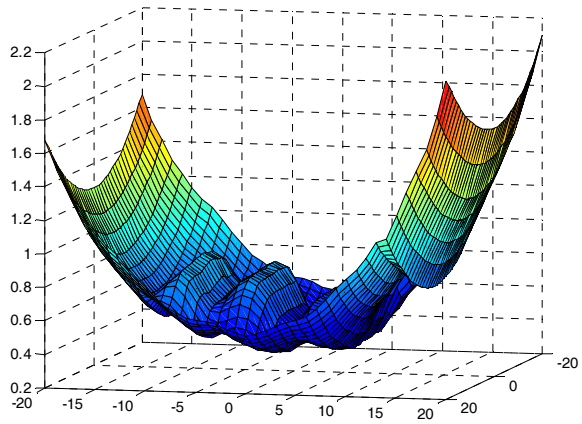

Figure 5: Wheel flat geometry in 3D

6 Results

The numerical contact model is used for wheel and rail interaction calculation and field measurement is used for validation. Also the Hertzian contact model is used for comparison.

Although the contact force is not a direct output from the interaction model, when wheel and rail is in contact the contact force can be obtained from the wheel motion:

$$\begin{cases} F_c = F_0 - M_w \ddot{u}_w & u_w - u_r - \min(h) > 0 \\ F_c = 0 & else \end{cases} \quad (14)$$

For Hertz contact, the roughness from the assumed running line is used. However, due to the finite size of the wheel, its centre trajectory is different from the wheel flat profile [3]. So-called curvature processing is used to determine the wheel centre trajectory. This is shown in

Figure 6. The wheel centre trajectory is used as the input roughness for the Hertz contact model. Moreover, the roughness input is also filtered using a two-dimensional mattress model to take account of contact patch effect [14].

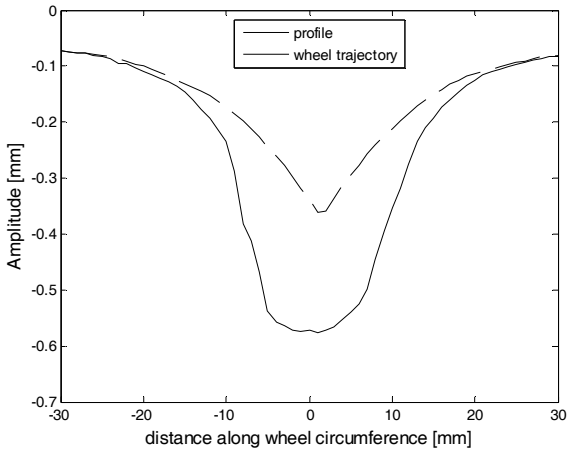

Figure 6 Wheel centre trajectory at wheel flat area

One full rotation of the wheel with flat spot is computed. The vehicle speed is 60.5 km/h and other parameters are listed in Table 1.

The contact force around wheel flat area is shown in Figure 7. It can be seen that these two contact models give quite similar results, except that the Hertzian contact model gives a higher peak force level. Also, it is noted that the Hertzian model gives strong double peak for the highest force level. This might be due to the rail oscillation on the contact spring. For the non-Hertzian model, since the contact stiffness is varying according to the contact geometry during the contact, it does not exhibit such behaviour.

The contact force spectrum in one-third octave bands is shown in Figure 8. This is computed from one full rotation of the wheel along the rail. The spectra from the two models are similar below 1 kHz since the track dynamics controls the response in this region. However, as the track system is the same, the difference between the two models around 1 kHz is evidently an effect of contact modelling.

The two contact models are compared with measured results from [12] in terms of vertical rail acceleration, as shown in Figure 9. The accelerometer was fixed in the mid span between two sleepers. As before, the measured acceleration of the rail corresponds to one rotation of the wheel. For the predictions, the response position is fixed on the rail as the wheel passes, in analogy to the experiment.

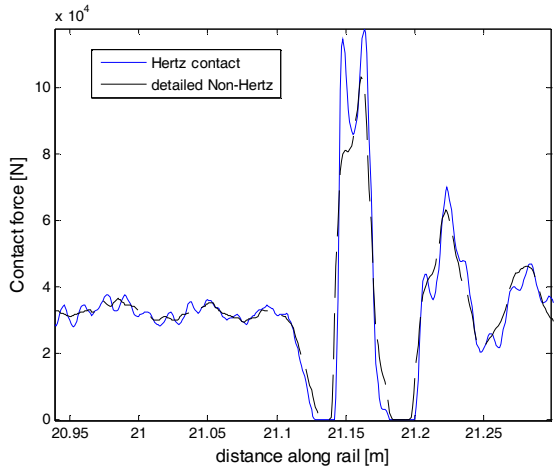

Figure 7 Contact force around wheel flat area along the rail

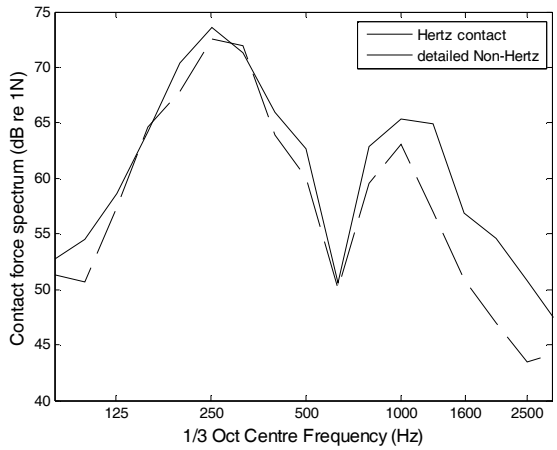

Figure 8 Contact force spectrum from one full rotation of the wheel with flat

Table 1 Wheel and rail parameters

Notation	Value	Units	Description
Vehicle			
V	60.5	km/h	Vehicle speed
M_w	600	kg	Wheel mass
F_0	33	kN	Vehicle load
Track			
I_r	20.18×10^{-6}	m^4	Second moment of area of rail
A_r	6.48×10^{-3}	m^2	Cross section area of rail
L	0.66	m	Sleeper spacing
M_s	133	kg	Half mass of sleeper
k_p	4.3×10^8	N/m	Rail pad stiffness
L_p	0.15	m	Width of rail pad
c_p	1.2×10^4	Ns/m	Pad damping
k_b	4×10^7	N/m	Ballast stiffness
c_b	3.98×10^4	Ns/m	Ballast damping

It is seen from Figure 9 that the two contact models predict similar results. As for the contact force results, the Hertzian contact model predicts a higher peak at around 1 kHz.

The simulation results are in agreement with the experiment in terms of peak and trough frequencies and average level of response. Especially, the detailed non-Hertzian contact model gives a very good match with the experiment at the peak at 1 kHz, both in frequency and amplitude. This improvement of the peak response prediction is because the variation of contact stiffness due to the contact geometry is considered. The difference is found to be less than 5 dB at other frequencies. This margin is acceptable considering that the contact position could vary, there might be errors in roughness measurement and in the acceleration results, etc.

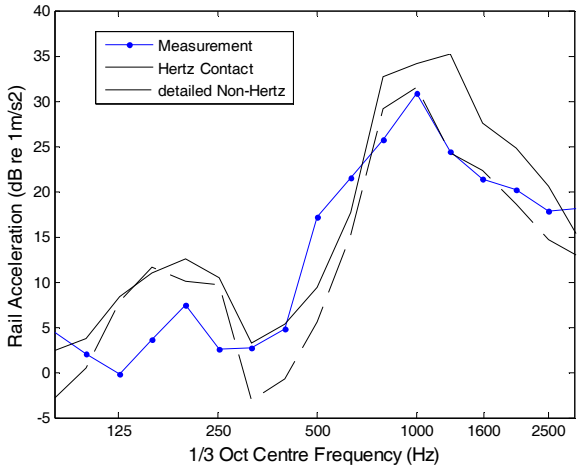

Figure 9 Rail acceleration at fixed position on rail during one wheel revolution, prediction and measurement

7 Conclusion

A detailed non-Hertzian contact model is considered in this paper to study wheel flat impacts. The requirements to use a Hertzian spring are not fulfilled due to the large variation of the geometry at the wheel flat area. A detailed numerical contact model is included dynamically in the wheel/rail interaction to predict the impact vibration due to wheel flat in time domain. The contact patch size is discretized adaptively at each time step to ensure all the contact points are included. Measured wheel flat geometry is used as the input where it is mapped to the profile in three dimensions. Good agreement is reached with experiments in terms of rail vibration, especially at the peak response. The difference is found to be less than 5 dB at other frequencies. This margin is acceptable considering uncertainties in the measurements.

In comparison, a Hertzian contact spring is also considered. These two models give similar results but an improvement is evident by taking account of the variation of contact stiffness.

Acknowledgments

The authors are grateful to SNCF for providing the measured data that was obtained as part Virginie Delavaud's PhD study.

References

[1] Thompson, D.J., *Railway Noise and Vibration. Mechanisms, Modelling and Means of Control*. 2008: Oxford, Elsevier Science. 506pp.

[2] Newton, S.G. and R.A. Clark, *An investigation into the dynamic effects on the track of wheelflats on railway vehicles.* Journal of Mechanical Engineering Science 1979. **21**(4): p. 287-297.

[3] Wu, T.X. and D.J. Thompson, *A hybrid model for the noise generation due to railway wheel flats.* Journal of Sound and Vibration, 2002. **251**(1): p. 115-139.

[4] Thompson, D.J., M.H.A. Janssens, and F.G.d. Beer, *TWINS: Track-Wheel Interaction Noise Software, theoretical manual (version 3)*, in *TNO report HAG-PRT-990211*. 1999, Delft.

[5] Baeza, L., et al., *Railway Train-Track Dynamics for Wheelflats with Improved Contact Models.* Nonlinear Dynamics, 2006. **45**(3): p. 385-397.

[6] Nielsen, J.C.O. and A. Igeland, *Vertical dynamic interaction between train and track influence of wheel and track imperfections* Journal of Sound and Vibration, 1995. **187**(5): p. 825-839.

[7] Croft, B., *The development of rail-head acoustics roughness*. 2009, University of Southampton.

[8] Remington, P. and J. Webb, *Estimation of wheel/rail interaction forces in the contact area due to roughness.* Journal of Sound and Vibration, 1996. **193**(1): p. 83-102.

[9] Kalker, J.J., *Three-Dimensional Elastic Bodies in Rolling Contact*. 1990: Kluwer Academic Publishers.

[10] Timoshenko, S.P. and J.N. Goodier, *Theory of Elasticity*. 3rd ed. 1970, New York: McGraw-Hill.

[11] Johnson, K.L., *Contact Mechanics*. 1987, Cambridge: Cambridge University Press. 452p.

[12] Delavaud, V., *Modélisation temporelle de l'interaction roue/rail pour une application au bruit de roulement ferroviaire, PhD Thesis*. 2011, ParisTech: Paris.

[13] Thompson, D.J. and P.J. Remington, *The effects of transverse profile on the excitation of wheel/rail noise.* Journal of Sound and Vibration, 2000. **231**(3): p. 537-548.

[14] Ford, R.A.J. and D.J. Thompson, *Simplified contact filters in wheel/rail noise prediction.* Journal of Sound and Vibration, 2006. **293**(3–5): p. 807-818.